The Design and Fabrication of an Autonomous Hybrid VTOL Aircraft

by

Amro A. Alshareef

Submitted to the
Department of Mechanical Engineering
in Partial Fulfillment of the Requirements for the Degree of

Bachelor of Science in Mechanical Engineering

at the

Massachusetts Institute of Technology

May 2020

Signature of Author ……………………………………………………………………...
Department of Mechanical Engineering
May 8, 2020

Certified by …………………………………………………………………………...
Srinivas (Sai) Ravela
Principal Research Scientist, MIT EAPS
Thesis Supervisor

Accepted by …………………………………………………………………………..
Anette Hosoi
Professor of Mechanical Engineering
Undergraduate Officer

The Design and Fabrication of an Autonomous Hybrid VTOL Aircraft

By

Amro Alshareef

Submitted to the Department of Mechanical Engineering
on May 8, 2020 in Partial Fulfillment of the
Requirements for the Degree of

Bachelor of Science in Mechanical Engineering

ABSTRACT

Low-cost Unmanned Aircraft Systems have proven to be extremely useful for tracking and mapping coherent atmospheric structures. These aircraft systems are often required to alternate between dynamic, non-uniform sampling and deterministic trajectories, which makes VTOL aircrafts especially suitable for these applications. Outlined is the process by which an autonomous VTOL aircraft weighing less than 10 kg and powered by a hybrid engine is designed and fabricated. The preliminary design of the aerodynamic shell is overviewed. Design requirements for the aircraft are then listed, followed by design and analysis of individual components and mechanisms within the structure in order to inform material selection. The fabrication process of the aircraft is then described, followed by the design and fabrication of a 4-axis CNC foam cutter needed to cut the aerodynamic surfaces of the aircraft out of EPP foam. Lastly, further work to be done on the CNC foam cutter and the Aircraft is listed.

Thesis Supervisor: Srinivas (Sai) Ravela
Title: Principle Research Scientist, MIT EAPS

Acknowledgements

Table of Contents

List of Figures

List of Tables

1. Introduction

The IcyQ project emerged from research experience developing and deploying autonomous unmanned aircraft systems (UAS) for environmental observation at the Earth Signals and Systems Group (ESSG) at MIT [1-5]. In prior work, low-cost UAS were rapidly demonstrated for tracking and mapping coherent atmospheric structures such as volcanic plumes and shallow clouds. Subsequently, systems to track wildlife, disaster reconnaissance, and mapping the retreat of Glacier were of interest. Currently, in an Office of Naval Research (ONR) award, aircrafts that rapidly change dynamic regimes are being developed.

There are a few common issues that emerge in the aforementioned applications. In most cases access to runways for takeoff and landing is difficult. The aircraft must therefore be small, and limits develop on the payload. Features such as undercarriages are eliminated, then batteries powering the aircraft become smaller. Batteries are selected as the power source to operate effectively in various sampling environments, as well as dynamic regimes. However, small batteries limit endurance, which typically must span hours, and further reduces range, which is typically required to be around 5-20 km. The aircraft must often transition from glider modes to agile behavior to respond and track environmental flow fields. For example, when observing wildlife, it is necessary to not frighten them. In other applications, the aircraft are often part of a closed loop observing system, gathering data to estimate parameters and states of environmental models. Numerous examples of other environmental applications exist that motivate our work [6]. In these applications, they may be called upon to implement varied and non-uniform sampling trajectories, in contrast to simple deterministic ones like a fixed, repetitive pattern.

Considering all these requirements, it is difficult to use battery-operated fixed-wing or multi-rotor (e.g. quadcopter) systems. However, a design that would address most of these issues is a Vertical Take-Off and Landing (VTOL) aircraft system that can transition from hover to forward flight and back and employs a gas-electric hybrid engine to provide the endurance. This architecture can enable range, endurance, agility, glide and other elements of performance that have been lacking in small unmanned aircraft systems for environmental observation. Presented here is the design and fabrication of such an aircraft and the instruments needed to fabricate it.

2. Background

The mechanical structure of the aircraft supports an aerodynamic shell designed by another undergraduate researcher in ESSG. The shell has a 3 m wingspan, with the wings incorporating a tapered leading and trailing edge, with a 4 degree angle of attack, a dihedral angle of 5 degrees, and a 0.95 m cross-section. The fuselage incorporates a nose-cone front with and a tapered tail cone, with a cylindrical center body to host the power plant and payload of the system. This fuselage is designed to be detachable from the wings, which are fixed via four support beams. The fuselage is also connected via a support beam to the tail of the aircraft, supporting two horizontal and a vertical stabilizer with control surfaces.
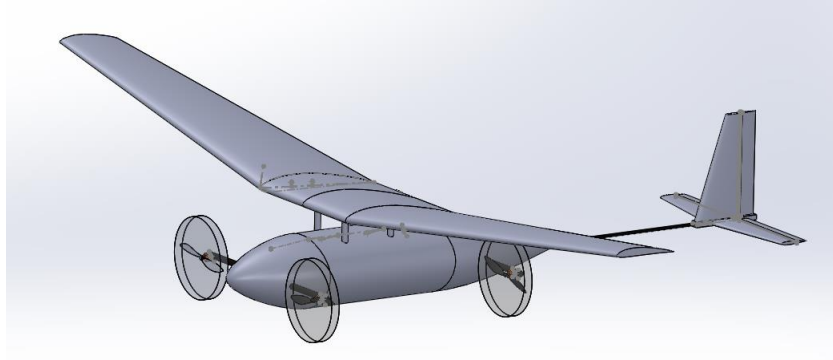
Figure 2-1: 3D visualization of the Aerodynamic surfaces of the aircraft

Figure 2-1 depicts the initial 3D model of the aerodynamic surfaces of the aircraft described above. Preliminary Computational Fluid Dynamics (CFD) testing on the model resulted in a drag coefficient for the wings of 0.09 at a flow speed of 30 m/s. The loads due to drag and lift informed the following design of the mechanical support structure and mechanisms controlling the aircraft.

3. Design of the Aircraft

3.1 Design Requirements

The primary objective of the system was to allow for both dynamic and agile movement, as well as hovering, stable flight for extended periods of time. Furthermore, the aircraft was to be detachable for easy compartmentalization, as it was to be readily transportable for operations in the field. The following design requirements, therefore, arose for the system:

1. The entire structure must be lighter than 10 kg, including payload, to increase the flight duration to fuel consumption ratio and maneuverability.
2. The propeller arms must rotate 90 degrees from propeller horizontal to vertical, allowing the system to transform between a VTOL to a forward-flight aircraft.
3. The Center of Gravity (CG) of the system must be at quarter cord for stable flight.
4. CG must be in line with motors in forward flight to prevent any destabilizing moments from affecting flight control.
5. The structure must be able to be disassembled into five sections, including a main fuselage, two wings sides, a wing center, and a tail section.

3.2 Structural Analysis and Validation

Due to the large size of the aircraft (3 m wingspan with a 2 m nose-to-tail length) along with its mass constraints, I determined that the ideal material for the mechanical structure was Carbon Fiber (CF) due to its strength to weight ratio. Figure 3-1 illustrates the simplified system model of the propeller support beam that was used to derive the desired CF tube size in order to minimize vibration and deflection under the loads experienced during flight.
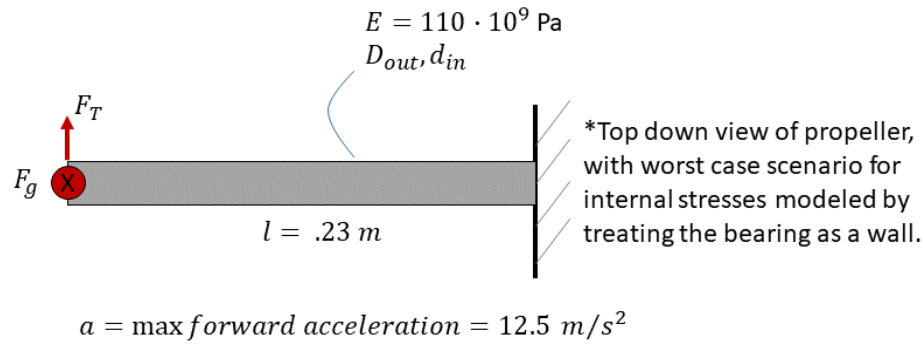
$E = 110 \cdot 10^9$ Pa
D_{out}, d_{in}

F_T

F_g

$l = .23\ m$

*Top down view of propeller, with worst case scenario for internal stresses modeled by treating the bearing as a wall.

$a = \max forward\ acceleration = 12.5\ m/s^2$

Figure 3-1: Propeller support beam model. The Young's modulus is that of 45° twined CF tubing. The maximum expected acceleration of the aircraft during forward flight is 'a'.

I made the following calculations in order to calculate the effective force acting on the propeller beam due to the weight of the aircraft along with the thrust of forward acceleration.

$$F_g = \frac{m * g}{4} = \frac{10_{kg} * 9.81_{m/s^2}}{4} = 24.525\ _N$$

$$F_T = \frac{m * a}{4} = \frac{10_{kg} * 12.5_{m/s^2}}{4} = 31.25\ _N$$

$$F_{resultant} = \sqrt{F_g{}^2 + F_T{}^2} = \sqrt{24.525^2 + 31.25^2} = 39.72\ _N$$

Using the second moment of inertia of the rod, I then calculated the deflection at the end of the rod as a function of the inner and outer diameters of the CF tube.

$$I = \frac{\pi * (D_{out}{}^4 - D_{in}{}^4)}{64}$$

$$\delta_{Prop} = \frac{F_{resultant} * l^3}{3 * E * I} = \frac{2.98 * 10^{-11}}{D_{out}{}^4 - D_{in}{}^4}$$

Using this equation, I generated a 3D plot in MATLAB with possible combinations of inner and outer CF tube diameters and the corresponding deflection associated with such a combination, as shown in Figure 3-2 below. The plot was filtered such that only realistic combinations remained, such as ones where the outer diameter was greater than the inner diameter, ones where the diameters were between zero and one inches, and ones that existed for commercial purchase.
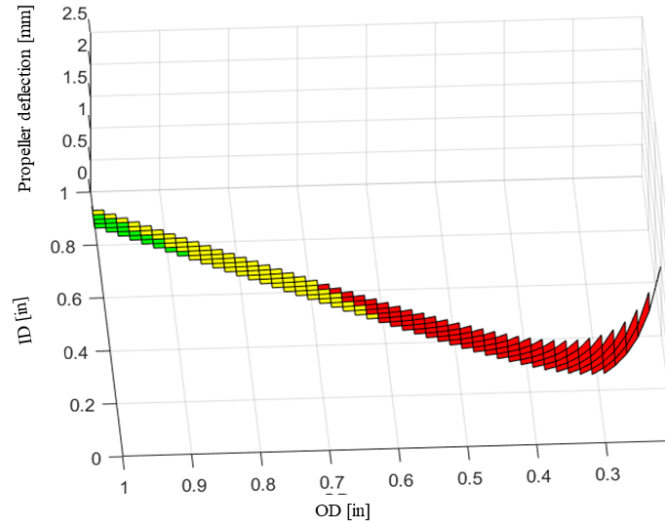
Figure 3-2: Combinations of inner and outer CF tube diameters and resulting beam deflection under associated flight loads. The OD and ID axis are in inches for easy cross-reference with US-based CF vendor catalogs. The green combinations represent ≤0.25 mm deflections, yellow represent between 0.25 and 0.5 mm deflections, and red represent >0.5 mm deflections.

In order to minimize beam deflection and eliminate the cost of having to source a custom sized CF tube, I chose a tube with an outer diameter of 0.875 in and an inner diameter of 0.75 in, which results in a propeller deflection of approximately 0.24 mm under max load.

The next structural members of concern were the four support beams connecting the fuselage to the wing. Figure 3-3 models the load on these beams. Note the axial load due to gravity was neglected because of the extremely lightweight foam composition of the wings compared to the high compressive strength of CF tubes. The only relevant load on the system is, therefore, the drag force on the wing.

*side view of wing-fuselage attachment, with the fuselage connection modeled as a wall. The wing is connected to the fuselage with 4 CF tubes.

F_{drag}

l

$E = 110 \cdot 10^9$ Pa
D_{out}, d_{in}

$v = \max flight\ speed = 30\ m/s$
$C_d = .09$
$A_{wing} = wing\ cross\ sectional\ area = .95\ m^2$
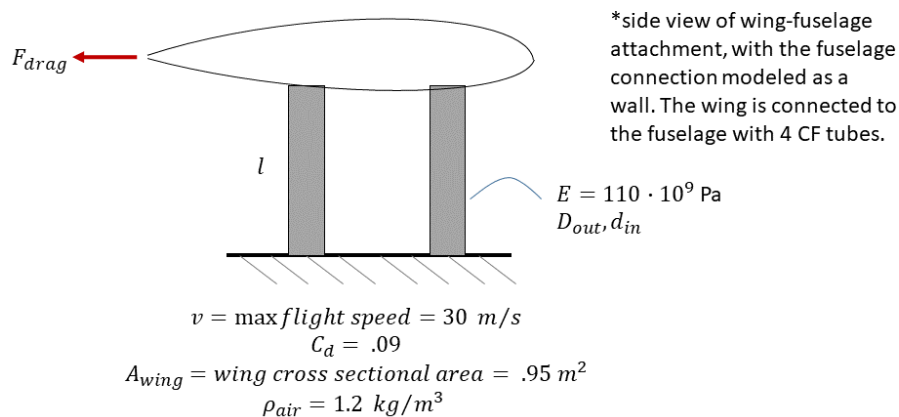$\rho_{air} = 1.2\ kg/m^3$

Figure 3-3: Simplified model of the wing-fuselage connection. The Young's modulus is that of 45° twined CF tubing. A_{wing} refers to the frontal cross-section of the wing, and v is the maximum expected velocity for the aircraft during flight.

12

I calculated the drag force using the coefficient of drag determined by the CFD simulations, and derived the resultant beam deflection, similarly to the propeller beam deflection. Due to the fact that 0.875 in by 0.75 in propeller tubes were already being purchased for the propeller beams, it was more cost efficient to add to a bulk purchase of the same tubing size rather than order a different size for the wing attachment. I, therefore, calculated the deflection for this tubing size.

$$F_{drag} = \frac{C_d * A_{wing} * \rho_{air} * v^2}{2} = 46.17_{N/beam}$$

$$I = \frac{\pi * \left(D_{out}^4 - D_{in}^4\right)}{64} = 4.966 * 10^{-9}{}_{m^4}$$

$$\delta_{beam} = \frac{F_{drag} * l^3}{3 * E * I} = .0001\ m = .1\ mm$$

At a negligible deflection of 0.1 mm, I chose the 0.875 in by 0.75 in tubing for the wing attachment. For the main structure in the aircraft fuselage, I chose square tubes due to the benefit of defined edges and flat surfaces for accessory attachments. The cost of square tube sizes does not vary noticeably, and 1 in tubing is a standard size for which connectors and mounts are readily available. Given that, I chose a thin walled, 1 in tube for the structural connecting members of the mechanical structure.

I designed the propeller motor mounts to be 3D printed with ABS plastic, which was accessible on campus, and mounted with epoxy on the ends of the propeller beams. I chose the design shown in Figure 3-4 in order to withstand the torque and upward force imparted on the mount by the motor, and to facilitate the aircraft's assembly process.
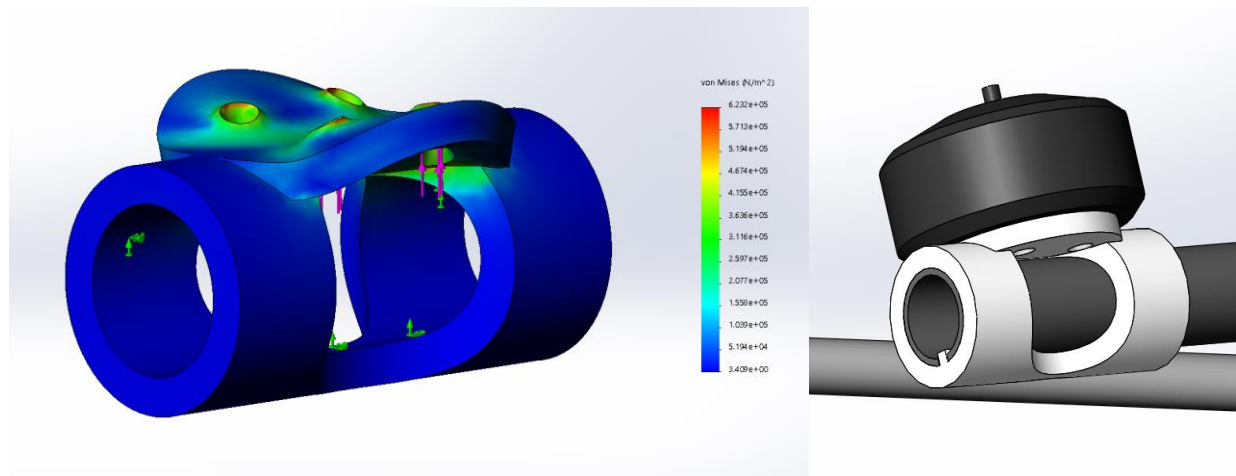
Figure 3-4: Model of the initial propeller motor mount design. SolidWorks FEA simulation was run with a 5 Nm torque on the screw holes in the motor central axis due to the motor torque imparted during rotation, and a 100 N upward force caused by the thrust force generated by the propellers.

The resultant deflection of the motor mount was less than 0.005 mm, with stress well below yield. This design was flawed, however, due to the inaccessibility of the motor screw holes after mounting. In order to be able to exchange motors and propellers easily, I modified the design to

that shown in Figure 3-5. Here, the design allows ready access to the screw holes for motor mounting after the mount is already epoxied, and it covers the end of the CF tube such that no dust, dirt, or moisture can accumulate inside the tube.
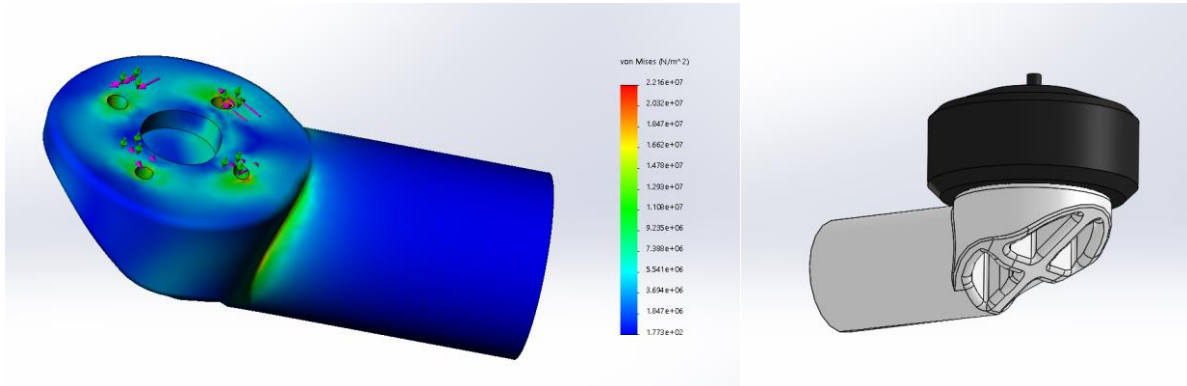

Figure 3-5: Model of the final propeller motor mount design. SolidWorks FEA simulation was run with similar parameters to those described in Figure 3-4.

This design still maintained a large radial cross-section in order to support the mount under the 5 Nm torque imparted by the motor without yielding. The resultant stress in the mount was, again, well below the yield stress of ABS plastic, and the deflection was less than 0.005 mm.

I initially designed the mechanism by which to rotate the propeller beams as a geared system with supporting ball bearings on either end of the structural base, as depicted on the left side of Figure 3-6. These ball bearings were fairly large and heavy, with a steel casing; they were, however, the only ball bearings available from our main vendor, McMaster, that fit the CF tube with a 0.875 in outer diameter. These bearings were also fairly expensive at approximately 15 USD apiece. For the rotation, I selected a DC motor with a hall effect sensor encoder and connected it via two custom aluminum gears to the propeller beam, as depicted in Figure 3-6. These gears can be waterjet using an OMAX waterjet on campus, as opposed to an extremely expensive and heavy commercial gear that would fit the CF tube.
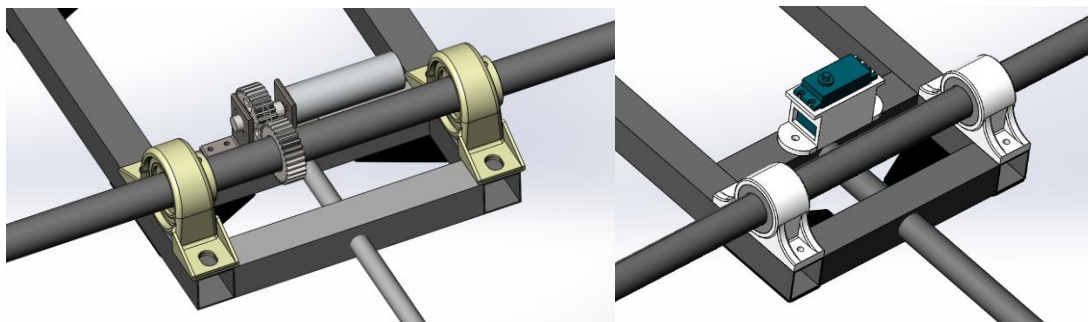
Figure 3-6: The rotation mechanism for the propeller beam that allows it to rotate between 0 and 90 degrees. On the left is the initial design of the mechanism, and on the right is the final redesigned mechanism.

Due to the fact that this motor mount rod does not have high radial velocities and only rotates between 0 and 90 degrees, however, a ball bearing is unnecessary and could instead be exchanged for a frictionless sleeve bearing. This is a more cost efficient design strategy, at about a dollar

apiece, and could be mounted with 3D printed mounts, cutting down costs from 30 USD to about 2 USD per beam, and making the system about 200 g lighter per bearing. Furthermore, the limited necessary range of motion and low torque required to rotate the beam was an indication that a lighter, cheaper servo connected to a carbon fiber bar linkage could be utilized. This eliminated the weight and need for fabrication of the aluminum gears, and exchanged the motors for limited range servos that are approximately 150 g lighter.

For the aerodynamic shell of the structure, I used 20 kg/m^3 EPP foam due to its light weight and shock absorption characteristics. Due to restrictions on the maximum sized foam blocks that can be cut in a foam cutter, the fuselage needed to be split into three sections and the wings into two segments. The fuselage also needed to be cored so the mechanical structure could be embedded within it, with openings for the all extruding support beams. This ultimately resulted in two halves of the fuselage, upper and lower, as shown in Figure 3-7. These two halves would be epoxied together, with a door chamber on each side of the top section that could be opened to access inside components, including the power plant.
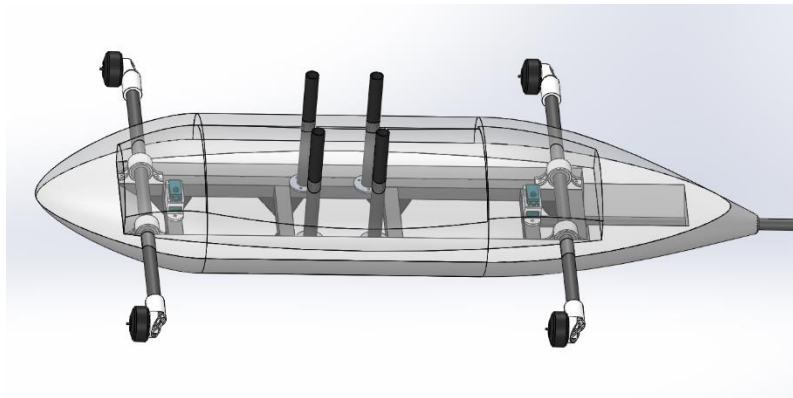

Figure 3-7**:** 3D model of the mechanical structure embedded in the aerodynamic foam shell. The cored inside and three subsections of the fuselage are indicated through the transparent upper shell.

3.3 Power Plant

In order to place the power plant for the aircraft in the system, I considered the variable mass of the fuel tank. The hybrid power plant consisted of an engine, a battery, and a fuel tank. The engine and the battery had a stable mass, but the fuel tank had a variable mass as the fuel in the tank depleted from an initial 2.5 kg. The Desired Center of Mass (CM) of the system, therefore, had to be achieved by the placement of the battery and the engine; the CM of the fuel tank needed to be placed coincident with that of the resultant aircraft so as to prevent movement of the aircraft CM through the duration of its flight, resulting in unstable control dynamics. I placed the CM of the system at the quarter cord of the wing, in line with the propeller propulsion force, and symmetrically between both propellers (X, Z, and Y-axis constraints in Figure 3-8, respectively) in order to prevent any undue moments on the system and for improved aerodynamic stability during flight.
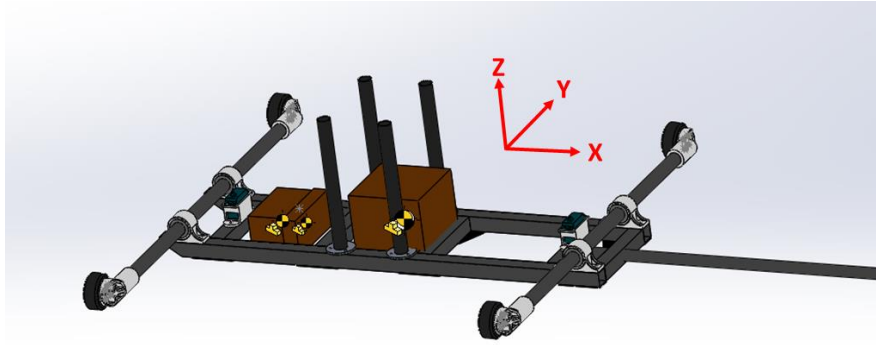
Figure 3-8: The final mechanical structure of the system with the CM of the battery, engine, and fuel tank indicated with yellow symbols and the CM of the system indicated in white.

The final aircraft, including the foam shell, mechanical support structure, motors and power plant, and 3 kg payload was approximately 9.8 kg. This aircraft included control surfaces on the wings and horizontal and vertical stabilizers, and was detachable into five segments: three wing sections, the tail section, and the main fuselage. The dimensions of the aircraft are indicated in meters in Figure 3-9.

Figure 3-9: 3D rendering of the final aircraft, including the mechanical structure and foam Aerodynamic surfaces. The units of the dimensions indicated are meters.

16

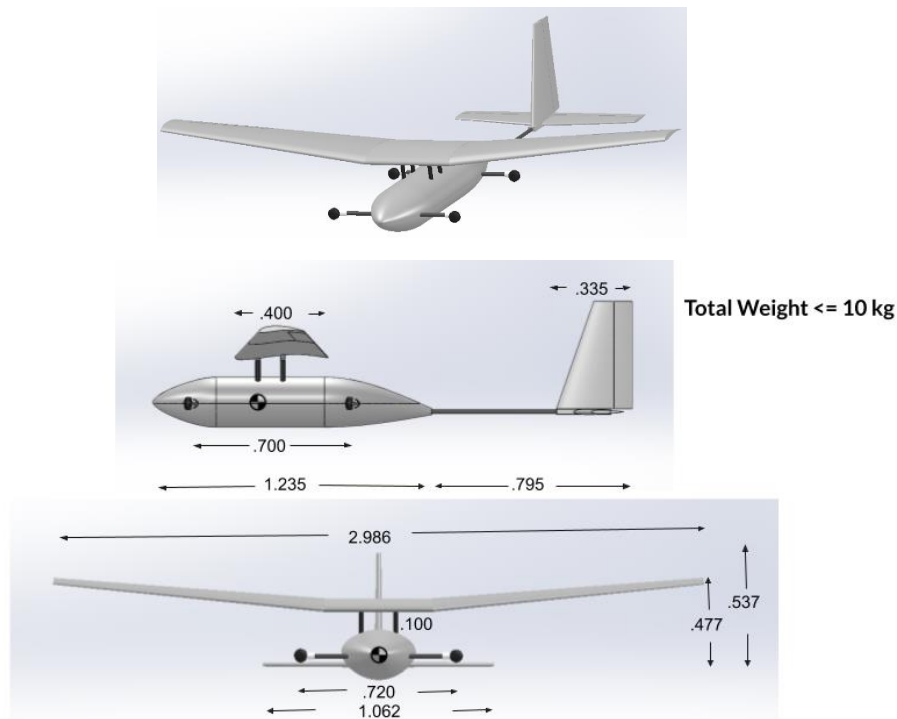# 4. Fabrication of the Aircraft

The Bill of Materials in Table 4-1 lists every component of the aircraft, including CF tubing, aluminum and delrin stock for beam supports, bearings, foam, and epoxy, along with the quantity needed of it and the vendor it was sourced from.

Component	Quantity	Description	Vendor
1 in CF square tube long	2	Square Carbon Fiber Tube 1" ID x 1.070" OD 72" length	Clearwater Composites
1 in CF square tube short	1	Square Carbon Fiber Tube 1" ID x 1.070" OD 36" length	Clearwater Composites
square tube connector plates	8	1" Square Tube Carbon Fiber Gusset 90° Tee	Dragon Plate
sleeve bearings	4	Dry-Running MDS-Filled Nylon Sleeve Bearing	Mcmaster
tail tube	1	0.590" X 3/4" Carbon Fiber Tube 72" Length	Clearwater Composites
prop tubes	2	3/4" X 7/8" Carbon Fiber Tube 96" length	Clearwater Composites
wing mounts stock	1	2" OD stock 6 in length	Mcmaster
wing tubes	3	0.313" X 0.394" Carbon Fiber Tube 72" Length	Clearwater Composites
control surface support	1	1mm Carbon Fiber Plate - Matte/Matte, 12x24	Clearwater Composites
20kg/m3 EPP Foam	5	Item no. EPPW20B1, Block 900x600x150mm (White)	Tower-Foam
Epoxy	1	3:1 Quart Medium Epoxy Hardener Kit (EPOX-635312)	US Composites

TABLE 4-1: Aircraft Bill of Materials

After using a horizontal bandsaw to cut the CF tubes to their respective dimensions as per the 3D model, I attached the square tubing using CF connector plates and rivets to hold them in place, with epoxy to permanently secure the structure. I turned the wing support beam mounts using 6061 Aluminum stock on a Computer Numerical Control (CNC) lathe. Next, I 3D printed bearing mounts and motor mounts using a Zortrax FDM printer with 1.75 mm ABS filament, which is what was readily available in open-access makerspaces on campus. These mounts, along with the aluminum wing support mounts, were bolted in place and epoxied to permanently secure. The resultant mechanical support structure is shown in Figure 4-10.

Figure 4-1: Mechanical structure of the aircraft assembled with epoxy curing.

The next step in fabrication was to cut the foam pieces that house the mechanical structure. The first option was to cut the foam using a CNC foam cutter on campus. I quickly dismissed this option, as I was advised that the only available cutter large enough to accommodate the sections of the aircraft was fairly unreliable. The second option I considered was to outsource the foam cutting, but this would have cost 5,500 USD with a four week lead time, and was therefore eliminated as a possibility. The third option considered was to purchase a CNC foam cutter for the lab, which would have a roughly two week lead time and cost approximately 5,000 USD. This, again, was too expensive and would take too long to arrive and set up. The final option I considered was to design and build my own 4-axis CNC foam cutter for the lab. This option would cost approximately 1,000 USD and would take roughly four to five weeks to complete. This option seemed to have the best cost to time ratio, with the added long-term benefit of having the lab's own, custom built foam cutter for future aircraft fabrication projects.

5. 4-axis CNC Foam Cutter

5.1 Design and Fabrication

Designing the cutter was fairly simple, as I could base my design on existing CNC cutters on the market. I designed the main framing for the four axes (X1, X2, Y1, and Y2) to be assembled in a jigging fashion. Each supporting aluminum member was modeled with either keys or slots to fit into other members. This key slot design was meant to ensure accuracy and ease during the welding process to fabricate each axis.
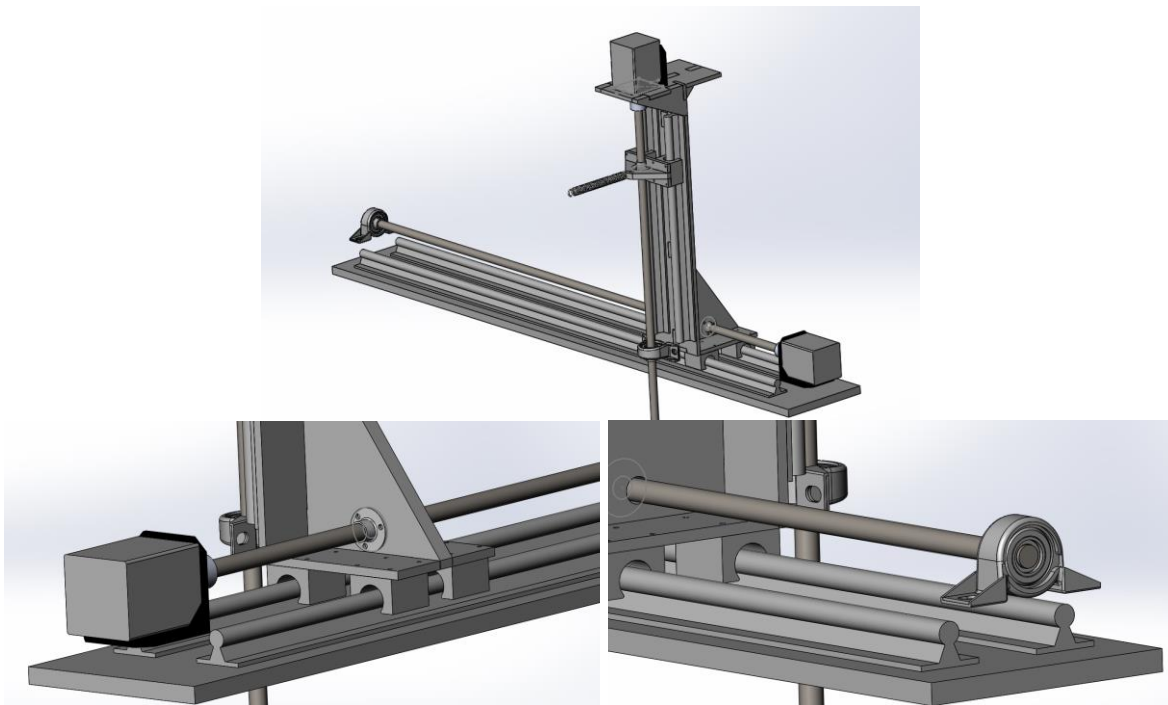

Figure 5-1: 3D model of the 4-axis CNC foam cutter.

Each axis was driven by a Nema 23 Stepper motor attached via a shaft coupling to a threaded rod. The Stepper motor was supported by a motor mount elevated to by 4 hex standoffs that I cut

down to the custom height that would please the motor output shaft in line with the driving axis. The X1 and X2 axes utilized a ½" - 13 threaded rod and a flanged nut to move the platforms connected to the Y1 and Y2 axes. Each axis slid along linear guide rails and was supported on the non-driven end by a frictionless ball bearing, also elevated to the proper height using 0.375 in stainless steel hex standoffs. I modified certain dimensions during the fabrication process as parts came in because railing dimensions were not specified online. The nichrome cutting wire attached to the spring on one side of the cutter and a mounting hole on the other to account for the varying wire length needed in the event of cuts with two varying cross-sections. Table 5-1, listing all of the parts sourced for the cutter and their quantities, was generated after all modeling of the system was completed.

ITEM	Quantity	Vendor
4 count Stepper Motor Mounting Bracket	1	AMAZON
8x12.7 mm Shaft coupling	2	
Nichrome Wire 28 Gauge	1	
20-1000 mm 2 Linear Rail guide	2	
stepper motor + motor controller+power supply	1	
400mm Travel Length Linear Stage Actuator DIY	2	
Estop	1	
14 gauge wire for power	1	
22 awg wire for low power connections	1	
limit switches	1	
Low-Profile Mounted Sealed Steel Ball Bearing	2	MCMASTER
Screw-Mount Nut	1	
Extension Springs with Hook Ends 3114T92	1	
Aluminum Sheet 1/4" Thick, 6" x 24"	2	
Aluminum Sheet 3/8" Thick, 12" x 48"	1	
Aluminum Sheet 1/2" Thick, 6" x 24"	1	
Steel Threaded Rod 1/2"-13, 3 Feet	2	
Male-Female Threaded Hex StandoffAluminum, 3/8" Hex Size, 2" Long, 8-32 Thread Size	8	
Steel Socket Head Screw, M6 x 1 mm Thread, 12 mm	1	
Steel Hex Nut M6 x 1 mm Thread	1	
Socket Head Screws Hex Drive 8-32 3/8"	1	
Male-Female Threaded Hex Standoff18-8 Stainless Steel, 3/8" Hex, 2" Long,10-32	4	

TABLE 5-1: Bill of Materials for the 4-axis CNC Foam Cutter.

After generating the 2D DXF files for all of the aluminum components of the structure, I loaded them into the OMAX waterjet software and cut them out of their respective aluminum stock. The resulting pieces are depicted in Figure 5-2, separated and assembled. As I had not yet known all of the dimensions of the railings and mounting sliders, I did not yet waterjet these holes out. If this design is implemented again, however, I suggest that the water jetting of the plates is done after all dimensions in regards to mounting are known, as this will eliminate the need for measuring and drilling holes later on.

Figure 5-2: Water-jet aluminum pieces for the foam cutter railing. On the right is shown how these pieces are to be jigged together for ease and accuracy of welding.

I welded the Aluminum railing using a water-cooled tig welder in the MIT D-Lab. This process involved scrubbing the oxidation layer that exists on the aluminum off using a clean stainless steel wire brush and cleaning the area to be welded with denatured alcohol. This step was critical to the strength of the weld joints as aluminum is especially susceptible to contaminants during the welding process. Figure 5-3 shows the resulting weld beads on the railing. A 0.25 in continuous weld bead was desired for the 0.25 in Aluminum plates.

Figure 5-3: Jigging and welding the aluminum plates for the CNC foam cutter railings.

In order to assemble the cutter, I initially used an angle grinder to cut the hardened steel railings down to size. I then measured, drilled, and tapped all the mounting holes for fasteners, and motor mounts. In order to mount the motor mounts and ball bearings, I also turned down the hex

standoffs to the precise heights needed to align the motor shafts, threaded rod, and bearings for each axis. After aligning and securing the flanged nuts, I then aligned the dual-linear railings on every axis with each other so as to prevent binding of the system during movement. The resultant four axes, consisting of two symmetric X-Y axis pairs, are shown in Figure 5-4.

Figure 5-4: Both sides of the 4-axis CNC foam cutter with mechanical fabrication and assembly fully complete.

5.2 Electrical and Software

The next step was to wire the electrical components of the system. The motors were wired according to the diagram in Figure 5-5 using 22 AWG wire. The dead-man switch and 24 Volt power supply were wired to their respective pins in Figure 5-7 using 14 AWG wire, accounting for the higher voltage running through the wire.
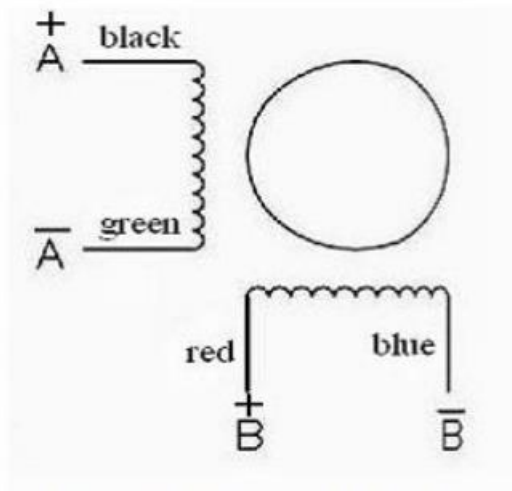

Figure 5-5: Stepper motor wiring diagram for the Nema 23 Stepper motors.

These wires had to be cut long enough to accommodate the travel of the axis, and connected to the motor controller depicted in Figure 5-6, which was powered by the 24V power supply at the V+ and V- pins, and connected to the main controller board via the signal interface.
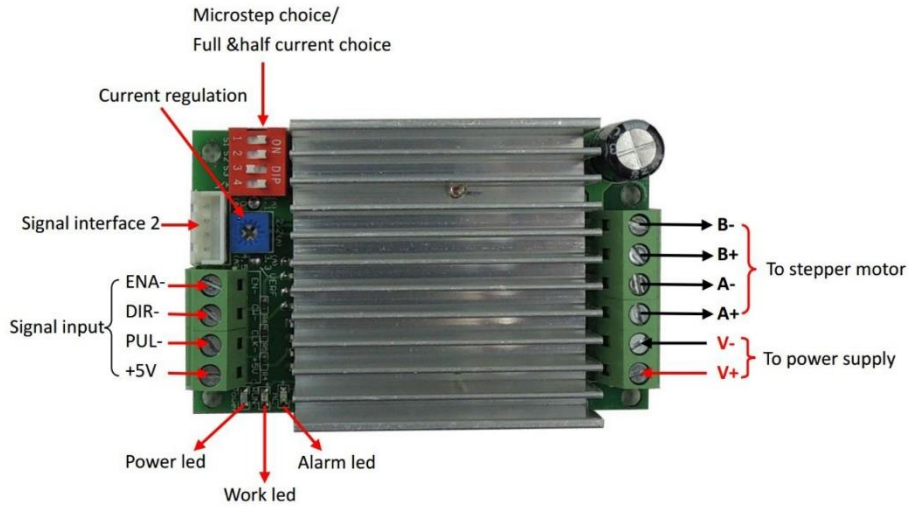
Figure 5-6: Stepper Motor controller that interfaces with the Mach3 Control board using the Artsoft Mach3 software

The main controller board interfaced with each of the motor axis via the signal output interface pins P2 through P9. The P10 through P14 pins allowed connection to limit switches on both ends of every axis and an emergency stop so that all axis could be shut down in the event of a malfunction or overdriving an axis. The hot wire connected to the 24 V pin on the board via a switch that I turned on when cutting in order to heat the wire. Lastly, the interface connected to a PC with the mach3 driver and software installed via the parallel port connector, and low-voltage functions of the board were powered from a USB connection to the PC.
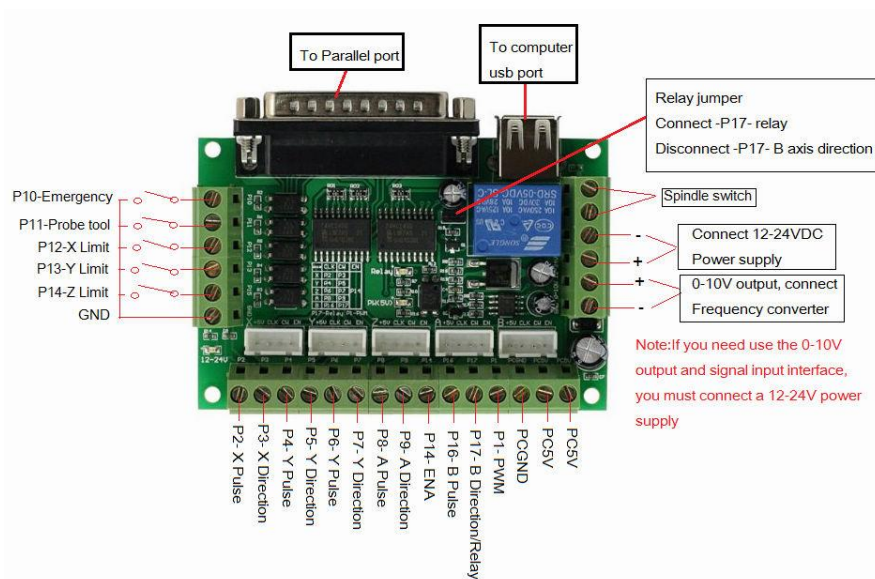

Figure 5-7: Main control board for the Mach3 software to interface with the control switches and each of the axis motors.

The control boards, power supply, and dead-man switch were all neatly organized in one control box shown in Figure 5-8. The wire connectors to each of the motor axes extended out of

the control box and wrapped around the outside of the cutter so as to not interfere with the movement of the cutter along its axes or possibly come in contact with the hot wire.
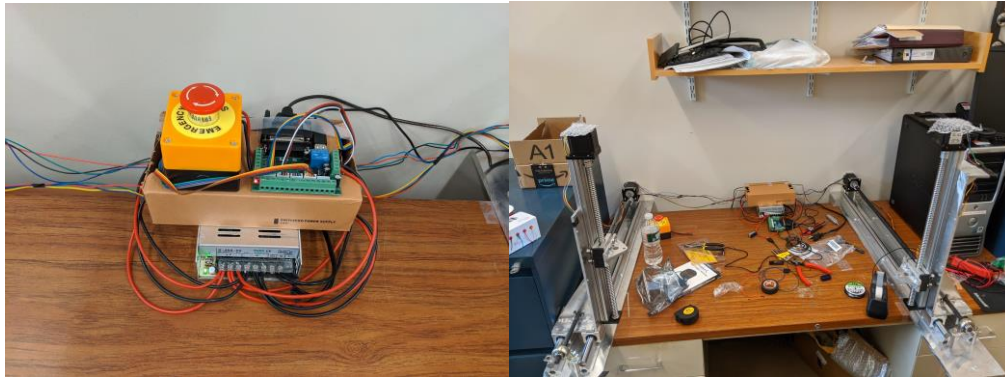

Figure 5-8: The control box for the cutter is shown on the left. On the right is the set-up for the cutter on a desk in the lab.

For the software, I initially attempted to install it on my laptop, but the driver would not install properly. After debugging, I realized that the driver required a 32-bit OS in order to install. With this knowledge, I installed a Virtual Machine (VM) running Windows XP, but that resulted in another problem: I did not have a parallel port to connect to the controller board. I then ordered a parallel port to USB converter, but that did not work as the controller board used every pin in the parallel port individually, while the converter connected some of the pins, thereby shorting them, because USB ports have fewer pin outputs than Parallel ports.

I then found an unused desktop that had a parallel port connection so that I could directly use the original cable, but I found that the VM did not support connection to the native parallel port. I thus needed a 32-bit system to be natively installed on the machine. I then found a spare Dell OptiPlex with a 32-bit Windows 7 installed on the drive. Next, I installed the software and the driver began working properly.

After this, I simply followed the setup procedures of the software itself and configured the motors and each axis. I used Jedicut, an open source 4-axis foam cutter G-code generator, in order to generate a simple G-code that would cut out a block outline of my lab team's name, "IcyQ". With this, I was then able to run G-code to cut out the foam piece in Figure 5-9 in honor of the team!

Figure 5-9: "IcyQ" letters cut out of EPP foam using the 4-axis CNC foam cutter.

6. Further work

Due to time being cut short as a result of Covid-19 epidemic, I was unable to complete this project. This involved all finishing touches on the cutter to increase its safety, usability, and reliability, cutting out the foam sections of the aircraft using the CNC cutter, and assembling all of the pieces together. The following includes further steps that should be taken in order to complete the project:

1. Limit switches should be installed on both sides of every axis of the 4-axis cutter to increase the safety of operation of the machine. After wiring, they need to be set up in the software so that they may be recognized if tripped.
2. The 4-axis cutter must be semi-permanently fixed to a stable platform and clamped down so that it does not vibrate during operation. Care must be taken to make sure they are exactly parallel and that the two attachment points of the spring and wire are the exact distance away from each other that is intended.
3. The wiring for the 4-axis cutter must be neatly wrapped and controlled so to prevent possible contact with the hot wire or interference with the movement of the machine.
4. The foam sections of the aircraft must be cut using the 4-axis foam cutter out of the EPP foam purchased. This involves generating 2D profiles of each of the foam sections to be cut and using Jedicut to generate the G-code for each foam piece. The foam can then be placed in between the two sides of the 4-axis cutter and the G-code runs on the machine.
5. Lastly, the foam pieces cut in step 4 must be epoxied onto the mechanical structure of the aircraft.

References

[1] Ravela, S., "Tractable Non-Gaussian Representations in Dynamic Data Driven Coherent Fluid Mapping", Handbook of Dynamic Data Driven Applications Systems: Springer, Cham, pp. 29–46, 2018.

[2] Ravela, S., "Cooperative Autonomous Observation of Volcanic Environments with sUAS", AGU Fall Meeting Abstracts, 2015.

[3] Ravela, S., "Cooperative Autonomous Observation of Coherent Atmospheric Structures using Small Unmanned Aircraft Systems", AGU Fall Meeting Abstracts, pp. B3230, 2014.

[4] Ravela, S., I. Sleder and T. Vigil, Tracking and Mapping Coherent Structures, International Conference on Computational Science, ICCS 2013

[5] Ravela, S., I. Sleder, and J. Salas, "Mapping Coherent Atmospheric Structures with Small Unmanned Aircraft Systems", Proc. AIAA Infotech@Aerospace (I@A): AIAA, 2013.

[6] Green, D., J. Hagon, C. Gomez, B. Gregory, "Using Low-Cost UAVs for Environmental Monitoring, Mapping, and Modelling: Examples from the Costal Zone", Costal Management: Global Challenges and Innovations (pp 465-501), Academic Press.